TOWARDS INVERSE VIRTUAL ANALOG MODELING

Alberto Bernardini

Dipartimento di Elettronica, Informazione e Bioingegneria,
Politecnico di Milano,
Piazza L. Da Vinci 32, 20133 Milano – Italy
alberto.bernardini@polimi.it

Augusto Sarti

Dipartimento di Elettronica, Informazione e Bioingegneria,
Politecnico di Milano,
Piazza L. Da Vinci 32, 20133 Milano – Italy
augusto.sarti@polimi.it

ABSTRACT

Several digital signal processing approaches, generally referred to as Virtual Analog (VA) modeling, are currently under development for the software emulation of analog audio circuitry. The main purpose of VA modeling is to faithfully reproduce the behavior of real-world audio gear, e.g., distortion effects, synthesizers or amplifiers, using efficient algorithms. In this paper, however, we provide a preliminary discussion about how VA modeling can be exploited to infer the input signal of an analog audio system, given the output signal and the parameters of the circuit. In particular, we show how an inversion theorem known in circuit theory, and based on nullors, can be used for this purpose. As recent advances in Wave Digital Filter (WDF) theory allow us to implement circuits with nullors in a systematic fashion, WDFs prove to be useful tools for inverse VA modeling. WDF realizations of a nonlinear audio system and its inverse are presented as an example of application.

1. INTRODUCTION

The term Virtual Analog (VA) modeling generally refers to a variety of approaches for digitally emulating the behavior of linear or nonlinear analog audio circuits [1, 2]. Such approaches can be roughly subdivided in two main classes [3]. The first class is the one of *gray box* modeling methods, which estimate the system starting from input-output measurements and a reference generic model; examples are Volterra-Wiener-Hammerstein models and modifications thereof [4, 5, 6], neural networks [7] and Legendre nonlinear filters [8]. The second class is the one of *white box* modeling techniques, which are based on the solution of the equations characterizing the actual audio circuit to be emulated; examples are state-space methods [9, 10], port-Hamiltonian methods [11] and Wave Digital Filters (WDFs) [12, 13]. Gray box modeling approaches are very general and, usually, once the parameters of the model have been derived, less computationally heavy than white box approaches. On the other hand, white box approaches are generally more accurate and do not require any estimation of the model parameters. The main purpose of VA modeling is to reproduce the output signal of real-world audio gear, e.g., distortion effects, synthesizers or amplifiers, finding an algorithm that ensures a good compromise between high accuracy and light computational weight. In this paper, however, we provide a preliminary discussion about how VA modeling can be exploited to estimate the input signal of an analog audio system, given the output signal and the parameters of the circuit. The scenario of interest is shown in Figure 1; assuming to know the parameters of System 1 and its time-domain output signal $y(t)$, we would like to recover the input signal $u(t)$ computing the output of System 2 given $y(t)$ as input. In the optimal case, System 2 is the exact inverse of System 1 and $\tilde{u}(t) = u(t)$. The capability of recovering the input signal $u(t)$ starting from the processed, eventually distorted, output signal $y(t)$ could be useful in various situations. As an example, effective techniques of the sort would allow us to perform *reamping* of sound signals from electric musical instruments, in order to change the applied effects or re-record with different amplifiers, when the "dry signal" is not available, but the originally used analog audio effect or amplifier is known.

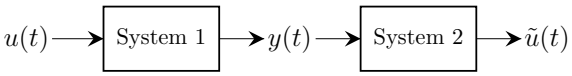

Figure 1: *Inverse system approach. If System* 2 *is the exact inverse of System* 1 *and the two systems share the same initial conditions, the signal* $\tilde{u}(t)$ *is a perfect estimate of the input signal* $u(t)$.

A possible strategy to attack this problem would be to use certain gray box approaches for modeling the system, e.g., Volterra-Wiener models, and then derive the corresponding inverse system, e.g., using functional or operatorial techniques [14, 15, 16]. An alternative idea, discussed in this paper, is to employ white box modeling approaches and resort to a theorem known in circuit theory [17] which, given a system represented as an electrical network, allows us to design its inverse. The theorem is based on the use of a theoretical 2-port circuit element called *nullor* [18]. Since recent theoretical advances in WDF theory allow us to design WDF models of circuits with nullors in a systematic fashion [19, 20], in this paper, we discuss how WDF principles can be exploited to derive digital realization of inverse systems, applying the theorem presented in [17]. Section 2 discusses the main aspects of the nullor-based inversion theorem. Section 3 recalls some recently developed techniques in WDF theory, such as a method for implementing circuits with nullors in the Wave Digital (WD) domain. As an example of application, Section 4 describes WDF realizations of a nonlinear audio clipper and its inverse. Section 5 concludes this paper and proposes possible future developments.

2. INVERSE SYSTEM DESIGN BASED ON NULLORS

2.1. Background on Nullors

A nullor [18], shown in Figure 2, is a theoretical 2-port linear circuit element composed of two other theoretical one-ports, called

nullator and norator. A *nullator* is a circuit element having zero current passing through it and zero voltage across its terminals, while a *norator* is characterized by an arbitrary current passing through it and an arbitrary voltage across its terminals.

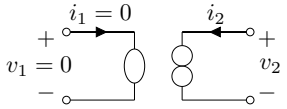

Figure 2: *A nullor composed of a nullator (represented with an ellipse) paired with a norator (represented with two contiguous circles).*

It follows that a nullor is characterized by the constitutive equation

$$\begin{bmatrix} v_1 \\ i_1 \end{bmatrix} = \begin{bmatrix} 0 & 0 \\ 0 & 0 \end{bmatrix} \begin{bmatrix} v_2 \\ i_2 \end{bmatrix} \quad , \tag{1}$$

where v_1 is the voltage across the nullator, v_2 is the voltage across the norator, i_1 is the current through the nullator and i_2 is the current through the norator.

Nullators, norators and nullors are often used to build macromodels of more complex multi-ports, such as 2-ports with controlled sources, operational amplifiers (opamps), transconductance amplifiers or transistors. For instance, an ideal opamp can be modeled using a nullor as shown in Figure 3, where v_{1+}, v_{1-} and v_{2+} are the potentials at the two input terminals and the output terminal of the opamp, respectively.

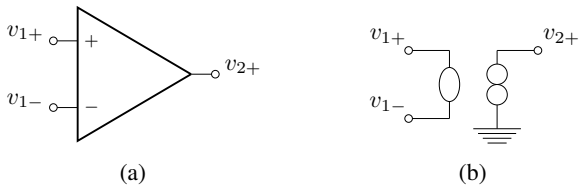

Figure 3: (a) *represents an ideal opamp, while* (b) *is an equivalent nullor-based representation of the same ideal opamp in* (a).

2.2. Inversion Theorem

Techniques for the analog realization of inverse systems have been explored in the mid-nineties [21, 22], especially with the purpose of developing methods for synchronizing chaotic systems [23]. A generalization of the inverse system approach used in [21, 22] was developed in [17], where a proven theorem is exploited for designing the inverse of a system that can be represented as an electrical circuit containing at least one nullor. The theorem presented in [17] is explained in the following.

Let us call the system to be inverted *master* and let us assume that it can be represented as in Figure 4(a); the system is constituted of a generic linear or nonlinear non-autonomous time-invariant network, and at least one nullator-norator pair connected to the network. A single input signal $u(t)$ is injected into the system using a voltage source, while the output signal $y(t)$ is the voltage measured across the norator. Let us then derive the so called *slave* referred to the master in Figure 4(a). The slave is obtained by replacing the input voltage source of the master with the norator and the norator with a voltage-controlled voltage source, whose control signal is $y(t)$; the resulting system is shown in Figure 4(b).

Another possible representation of a master system is reported in Figure 5(a); the system is analogous to the one in Figure 4(a), except that the output signal $y(t)$ is the current through the norator. The corresponding slave is represented in Figure 5(b), where the input voltage source of the master has been replaced with the norator and the norator with a current-controlled current source, whose control signal is $y(t)$.

Given the circuits in Figure 4 and in Figure 5, the following theorem enounced and proved in Section 3 of [17] holds; the theorem is here slightly reworded for the sake of clarity.

Theorem 1. If the two nonlinear dynamical systems in Figure 4 have unique bounded solutions, then, for any pair of signals $u(t)$ and $y(t)$, the slave in Figure 4(b) is the inverse of the master in Figure 4(a). This means that for any input signal $u(t)$ and every initial state vector $\mathbf{x}(0)$ for the master, there is an initial state vector $\tilde{\mathbf{x}}(0)$ for the slave such that $\tilde{u}(t) = u(t)$. The same holds for the master and the slave in Figure 5.

Similar results can be obtained when the input signal $u(t)$ is a current source, but they are not discussed here, since current sources are less common in audio circuits. A very common scenario, instead, is the one in which no nullors are present in the master system to be inverted, as in Figure 6(a), where the output signal $y(t)$ is the difference of potentials at two generic terminals (C and D) of the nonlinear network. It turns out that every circuit can be augmented with a nullor without altering its behavior [17]. In fact, since the series of a nullator and a norator is equivalent to an open circuit, the system in Figure 6(b) is characterized by exactly the same behavior of the one in Figure 6(a). It follows that the same procedure applied to the system in Figure 4(a) to derive its inverse can now be applied to the master in Figure 6(b), obtaining the corresponding slave in Figure 6(c). Hence, according to *Theorem 1*, the system in Figure 6(c) is the inverse of the system in Figure 6(a). Similarly, let us consider the system without nullors in Figure 7(a) whose output signal $y(t)$ is a current. Since the parallel of a nullator and a norator is equivalent to a short circuit, the system in Figure 7(b) is interchangeable with the system in Figure 7(a). It follows that the same procedure applied to the system in Figure 5(a) to derive its inverse can now be applied to the master in Figure 7(b), obtaining the corresponding slave in Figure 7(c). Hence, according to *Theorem 1*, the system in Figure 7(c) is the inverse of the system in Figure 7(a).

3. BRIEF OVERVIEW ON WDF MODELING

3.1. Basic WDF Principles

The WD modeling of a system is based on a port-wise consideration of the reference equivalent circuit and a linear transformation of Kirchhoff port variables into WD variables at each port, as the following [12]

$$a = v + Zi \quad , \quad b = v - Zi \quad , \tag{2}$$

where v is the port voltage, i is the port current, a is the incident wave, b is the reflected wave and Z is a scalar free parameter (port resistance). Variables defined in (2) are the so called *voltage waves* [12], however other kinds of waves with different units of measure [20] or more than one free parameter [24, 25] can be defined. The inverse relation of (2) is

$$v = (a + b)/2 \quad , \quad i = (a - b)/(2Z) \quad . \tag{3}$$

Figure 4: (a) *shows a nonlinear non-autonomous system with at least one nullor (the master). The input signal* $u(t)$ *is a voltage source, while the output signal* $y(t)$ *is the voltage across the norator.* (b) *shows the inverse system (the slave) of the one in* (a). *Letters* A, B, C, D, E *and* F *indicate the same nodes of the nonlinear network both in* (a) *and* (b).

Figure 5: (a) *shows a nonlinear non-autonomous system with at least one nullor (the master). The input signal* $u(t)$ *is a voltage source, while the output signal* $y(t)$ *is the current through the norator.* (b) *shows the inverse system (the slave) of the one in* (a). *Letters* A, B, C, D, E *and* F *indicate the same nodes of the nonlinear network both in* (a) *and* (b).

Substituting (3) in the constitutive equations of circuit elements and then expressing b as a function of a, WD *scattering relations* at each port are found. When modeling most linear one-ports, e.g., resistors, resistive sources, capacitors and inductors, in the WD domain, it is possible to spend the free parameter Z in order to eliminate the instantaneous dependence between a and b; this process is called *adaptation*. In WD structures, the connection networks that connect circuit elements (e.g., in series, in parallel or according to more complex constraints) are implemented using N-port scattering junctions, called *adaptors*. A scattering junction is characterized by scattering matrices that satisfy the following general equation

$$\mathbf{a} = \mathbf{S}\mathbf{b} \ , \tag{4}$$

where $\mathbf{a}$ is the vector of waves reflected from the junction (and incident to the elements or the other adaptors of the WD structure connected to the junction), while $\mathbf{b}$ is the vector of waves incident to the junction (and reflected from the elements or the other adaptors connected to the junction). For a detailed description of basic linear WD elements and adaptors the reader is referred to [12]. Instead, a brief discussion on the modeling of WD structures with nonlinearities, nonreciprocal multi-ports and complex topologies is provided in the following subsection.

3.2. Recent Advances in WDF Theory

Despite the idea of using WD structures for sound synthesis through physical modeling and Virtual Analog modeling dates back to the nineties [1, 26], a considerable effort has been made in the last few years to enlarge the class of audio circuits that can be modeled in the WD domain. In particular, WD models of linear and nonlinear circuit elements, such as operational amplifiers [27, 28, 19, 29, 30], nonlinear transformers [31], diodes [27, 32, 33, 34], vacuum tubes [35, 36] and transistors [37, 38, 39, 40, 41], that were not considered in traditional WDF theory [12] have been discussed. Moreover, novel design strategies for implementing $\mathcal{R}$-type WD adaptors describing arbitrary reciprocal [42] or nonreciprocal [20] connection networks have been developed. Dynamic circuits with up to one nonlinear element can be implemented using WD structures without Delay-Free-Loops (DFLs), i.e., fully *explicit* [43, 26, 34]. Although this desirable property is not maintained when we deal with circuits with multiple nonlinearities, some novel approaches have been recently presented for solving this kind of circuits using the K method [44, 38] or iterative techniques [45, 40, 46, 47, 48].

In the context of this article, the modeling of nullors in the WD domain is of particular interest. Nullators, norators and nullors are singular elements [18]. It follows that they cannot be modeled as other circuit elements in the WD domain using separable blocks characterized by local scattering relations. However, systematic methods developed in [19, 20] can be adopted to model circuits with nullors in the WD domain. Such methods are based on the Modified Nodal Analysis [49] and they allow us to derive WD realizations of nonreciprocal connection networks embedding both topological information and nullors; the result are special $\mathcal{R}$-type WD adaptors which are neither pseudolossless nor reciprocal [20].

In the next Section, as an example, we will show how both an audio clipper with one nonlinearity and its nullor-based inverse can be implemented in the WD domain in an explicit fashion.

4. WDF REALIZATIONS OF A NONLINEAR AUDIO CLIPPER AND ITS INVERSE

4.1. Circuit of the Audio Clipper and Design of its Inverse

The circuit of the nonlinear diode-based audio clipper that we will consider is shown in Figure 8(a). The input signal $u(t)$ is the voltage supplied by the voltage source. The output signal $y(t)$ is the voltage across the resistor with resistance R_{out}. The circuit is composed of: five linear resistors with resistances R_{p}, R_{m}, R_{fl}, R_{fh} and R_{out}; two linear capacitors with capacitances C_{p} and C_{m}; and two nonlinear diodes, D_1 and D_2, in antiparallel. The two diodes are

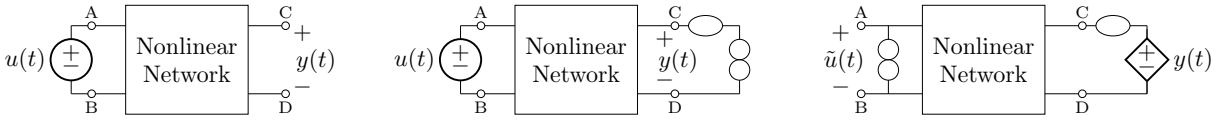

Figure 6: (a) *shows a nonlinear non-autonomous system without nullors (the master). The input signal $u(t)$ is a voltage source and the output signal $y(t)$ is a voltage.* (b) *shows a system equivalent to the one in* (a) *augmented with a nullator-norator pair.* (c) *shows the inverse system (the slave) of the one in* (a).

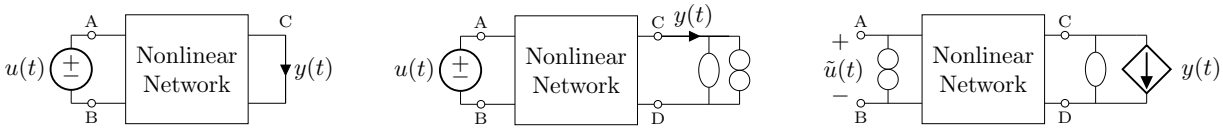

Figure 7: (a) *shows a nonlinear non-autonomous system without nullors (the master). The input signal $u(t)$ is a voltage source, while the output signal $y(t)$ is a current.* (b) *shows a system equivalent to the one in* (a) *augmented with a nullator-norator pair.* (c) *shows the inverse system (the slave) of the one in* (a).

identical and both characterized by the Shockley diode model

$$i_{\mathrm{d}} = I_{\mathrm{s}}(e^{v_{\mathrm{d}}/(\eta V_{\mathrm{th}})} - 1) \ , \tag{5}$$

where i_{d} is the current passing through the diode, v_{d} is the voltage across the diode, I_{s} is the saturation current, η is the ideality factor of the exponential junction and V_{th} is the thermal voltage. A detailed list of the circuit parameters and the corresponding values is reported in Table 1. For the purpose of designing an inverse

Table 1: *Parameters of the Audio Clipper Circuit*.

Param.	**Value**	**Param.**	**Value**	**Param.**	**Value**
(ηV_{th})	26 mV	C_{p}	1 pF	R_{p}	39 kΩ
I_{s}	2.52 nA	C_{m}	3.9 nF	R_{m}	22 kΩ
R_{out}	150 kΩ	R_{f1}	50 kΩ	R_{f2}	50 kΩ

audio clipper, given the system in Figure 8(a), we add a nullor to the circuit. In fact, as explained in Subsection 2.2, a circuit can always be augmented with a nullator-norator pair obtaining another circuit equivalent to the original one. Figure 8(b) shows the audio clipper circuit with a series of a nullator and a norator from node C to ground which has exactly the same behavior of the one in Figure 8(a). Starting from the master in Figure 8(b), we get the corresponding slave in Figure 9(a), according to the Theorem in Subsection 2.2. Figure 9(b) shows an alternative representation of the inverse nonlinear audio clipper, where the nullor is replaced by an opamp. It is worth recalling that, if the opamp is characterized by the ideal nullor-based model shown in Figure 3, the circuit in Figure 9(b) is totally equivalent to the circuit in Figure 9(a); if a non-ideal opamp model is considered, instead, the circuit in Figure 9(b) is an approximation of the "exact inverse" in Figure 9(a).

4.2. Design of WD Structures and Simulation Results

A possible WD realization with no DFLs of the nonlinear audio clipper in Figure 8(a) is shown in Figure 10(a). WD blocks (elements or junctions) including a "T-shaped" symbol at one port are adapted at that port. As far as the WD modeling of the circuit elements is concerned, linear elements are all adapted according to traditional WDF principles [12]. In particular, the wave reflected from a resistor with resistance R at the nth port of an adaptor is $b_n = 0$ during the whole simulation, provided that the adaptation condition $Z_n = R$ is satisfied. The reflected wave from a capacitor with capacitance C at sampling step k, instead, is given by $b_n[k] = a_n[k-1]$, provided that the bilinear transform is applied to discretize the time derivative and the adaptation constraint $Z_n = T_s/(2C)$ is set, where $F_{\mathrm{s}} = 1/T_{\mathrm{s}}$ is the sampling frequency. The voltage source is augmented with a negligible small series resistances $R_{\mathrm{e}} = 1\ \mu\Omega$; the reflected wave is computed as $b[k] = u(kT_s)$ with $Z_5 = R_{\mathrm{e}}$. The pair of antiparallel diodes is treated as a one-port. Since it is nonlinear, such a one-port cannot be adapted and, according to [27, 33, 39], its WD mapping can be expressed as

$$b = \mathrm{sgn}(a)F(|a|, Z, I_{\mathrm{s}}, \eta, V_{\mathrm{th}}) \ , \ \text{with} \tag{6}$$

$$F(a, Z, I_{\mathrm{s}}, \eta, V_{\mathrm{th}}) = a + 2ZI_{\mathrm{s}} - 2\eta V_{\mathrm{th}} W\left(\frac{ZI_{\mathrm{s}}}{\eta V_{\mathrm{th}}} e^{\frac{ZI_{\mathrm{s}}+a}{\eta V_{\mathrm{th}}}}\right) \ ,$$

where W is the Lambert function. The connection network of the circuit in Figure 8(a) is reciprocal, hence it is implemented using an interconnection of two reciprocal WD junctions [42]: the parallel adaptor $\mathcal{P}_1$ and the $\mathcal{R}$-type adaptor $\mathcal{R}_1$. The standard 3-port parallel adaptor is realized as discussed in [12], while the 8-port $\mathcal{R}$-type adaptor is characterized by a scattering matrix $\mathbf{S}_{\mathcal{R}_1}$, which can be formed as [42]

$$\mathbf{S}_{\mathcal{R}_1} = 2\mathbf{Q}^T\left(\mathbf{Q}\mathbf{Z}^{-1}\mathbf{Q}^T\right)^{-1}\mathbf{Q}\mathbf{Z}^{-1} - \mathbf{I}_8 \ , \tag{7}$$

where $\mathbf{I}_8$ is the 8×8 identity matrix, $\mathbf{Z} = \mathrm{diag}[Z_1, \ldots, Z_8]$ is the diagonal matrix of port resistances (port numbering follows the convention in Figure 10(a)) and $\mathbf{Q}$ is the fundamental cut-set matrix characterizing the connection network and given by

$$\mathbf{Q} = \begin{bmatrix} -1 & 0 & 0 & 1 & 1 & 0 & 0 & 0 \\ 1 & -1 & 0 & 0 & 0 & 1 & 0 & 0 \\ 0 & 1 & 1 & 0 & 0 & 0 & 1 & 0 \\ 0 & 0 & -1 & -1 & 0 & 0 & 0 & 1 \end{bmatrix} .$$

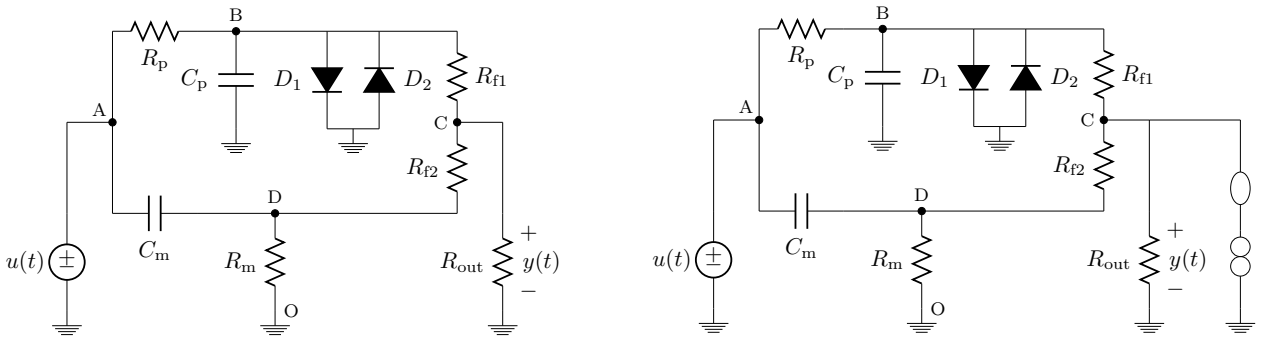

Figure 8: (a) *shows the circuit of the nonlinear audio clipper.* (b) *shows a circuit equivalent to the one in* (a) *augmented with a nullor.*

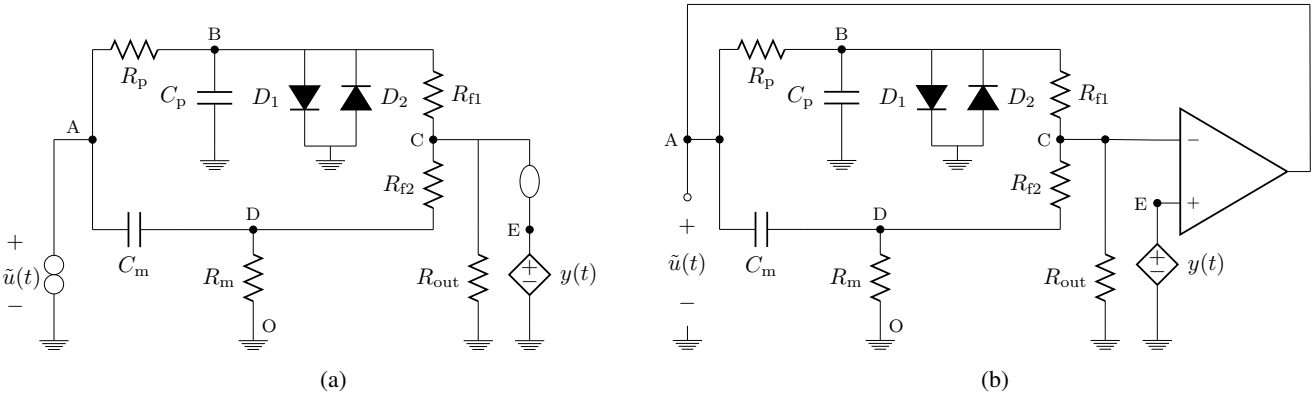

Figure 9: (a) *shows the circuit of the inverse nonlinear audio clipper.* (b) *shows an alternative representation of the inverse nonlinear audio clipper where the nullor is replaced by an opamp. If the opamp is characterized by the ideal nullor-based model in* Figure 3, *the circuit in* (b) *is fully equivalent to the circuit in* (a).

Port 6 of $\mathcal{R}_1$ is made reflection-free by setting the 6th diagonal entry of the scattering matrix equal to zero. The expression of the adaptation constraint on Z_6 is not reported here for the sake of brevity; however, given the circuit parameters in Table 1, we get the constraint $Z_6 = 27110\,\Omega$.

As far as the inverse audio clipper in Figure 9(b) is concerned, a possible WD realization with no DFLs is shown in Figure 10(b). The elements and the 3-port parallel adaptor $\mathcal{P}_2$ are implemented in a similar fashion to the previous case; the $\mathcal{R}$-type adaptor $\mathcal{R}_2$, instead, differs from $\mathcal{R}_1$, as it is a WD realization of a non-reciprocal connection network embedding a nullor. According to [20], the scattering matrix $\mathbf{S}_{\mathcal{R}_2}$ of $\mathcal{R}_2$ is given by

$$\mathbf{S}_{\mathcal{R}_2} = 2\tilde{\mathbf{A}}_\mathrm{p}^T\,[\mathbf{I}_5\ \ \mathbf{0}]\,\tilde{\mathbf{X}}_0^{-1}[\mathbf{I}_5\ \ \mathbf{0}]^T\,\tilde{\mathbf{A}}_\mathrm{p}\mathbf{Z}^{-1} - \mathbf{I}_8\ , \qquad (8)$$

where $\mathbf{I}_5$ is the 5×5 identity matrix, $\mathbf{0}$ is a column vector of five zeros, $\mathbf{Z} = \mathrm{diag}[Z_1, \ldots, Z_8]$ is a diagonal matrix of port resistances (port numbering follows the convention in Figure 10(b)), $\tilde{\mathbf{X}}_0$ is the 6×6 matrix obtained removing the jth row ($1 \leq j \leq 7$) and the jth column of $\mathbf{X}_0$ in Figure 11, while $\tilde{\mathbf{A}}_\mathrm{p}$ is the 5×8 matrix obtained removing the jth column of $\mathbf{A}_\mathrm{p}$ in Figure 11. Port 1 of $\mathcal{R}_2$ is adapted by setting $Z_1 = (Z_3Z_5Z_7)/(Z_3Z_5 + Z_3Z_6 + Z_3Z_7 + Z_3Z_8 + Z_6Z_8)$.

The accuracy of the designed WDFs is verified comparing the output signals with those obtained from a Spice implementation and noting a good matching. One of such tests is reported in Figure 12. WD simulations are performed with a sampling frequency $F_\mathrm{s} = 44100$ Hz. Figures 13, 14 and 15 show some further results of the WD implementations of the master and the slave in Figure 10, when the input signal is a sinusoid, a square wave and a white noise, respectively. Detailed parameters of the input are specified in the captions. We notice that inversion works pretty well for each input signal choice, as $\tilde{u}(t)$ always closely matches $u(t)$. More precisely, let us define the absolute value of the estimation error as $\epsilon(t) = |\tilde{u}(t) - u(t)|$, and then derive its mean $\bar{\epsilon}$ and its maximum value ϵ_max. We get: $\bar{\epsilon} = 1.5 \times 10^{-11}$ V and $\epsilon_\mathrm{max} = 2.5 \times 10^{-11}$ V in the sinusoidal input case; $\bar{\epsilon} = 2.7 \times 10^{-11}$ V and $\epsilon_\mathrm{max} = 1.1 \times 10^{-10}$ V in the square wave case; $\bar{\epsilon} = 1.4 \times 10^{-11}$ V and $\epsilon_\mathrm{max} = 3.6 \times 10^{-11}$ V in the white noise case.

5. CONCLUSIONS AND FUTURE WORK

We discussed a general approach for the design and the WDF realization of the inverse of any input-output audio system that can be described using electrical equivalents. It is worth pointing out that the presented approach works properly only when we deal with invertible nonlinearities and that numerical problems may occur when nonlinear functions to be inverted are very steep. Future research work would be desirable for extending such an approach to

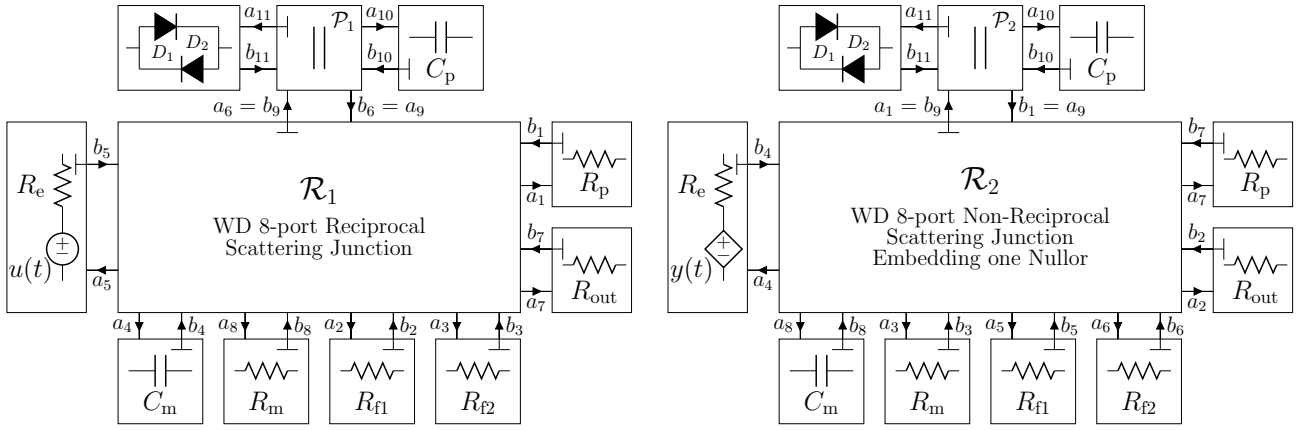

Figure 10: (a) *WDF implementing the nonlinear audio clipper*; (b) *WDF implementing the inverse nonlinear audio clipper*.

$$\mathbf{X}_0 = \begin{bmatrix} G_1+G_2+G_3+G_4 & 0 & -G_1 & -G_2 & -G_3 & -G_4 & 1 \\ 0 & G_7+G_8 & -G_7 & 0 & -G_8 & 0 & -1 \\ -G_1 & -G_7 & G_1+G_5+G_7 & -G_5 & 0 & 0 & 0 \\ -G_2 & 0 & -G_5 & G_2+G_5+G_6 & -G_6 & 0 & 0 \\ -G_3 & -G_8 & 0 & -G_6 & G_3+G_6+G_8 & 0 & 0 \\ -G_4 & 0 & 0 & 0 & 0 & G_4 & 0 \\ 0 & 0 & 0 & -1 & 0 & 1 & 0 \end{bmatrix} \quad \mathbf{A}_\mathrm{p} = \begin{bmatrix} -1 & -1 & -1 & -1 & 0 & 0 & 0 & 0 \\ 0 & 0 & 0 & 0 & 0 & 0 & -1 & 1 \\ 1 & 0 & 0 & 0 & -1 & 0 & 1 & 0 \\ 0 & 1 & 0 & 0 & 1 & 1 & 0 & 0 \\ 0 & 0 & 1 & 0 & 0 & -1 & 0 & -1 \\ 0 & 0 & 0 & 1 & 0 & 0 & 0 & 0 \end{bmatrix}$$

Figure 11: Matrices needed for deriving the scattering matrix of $\mathcal{R}$-type adaptor $\mathcal{R}_2$.

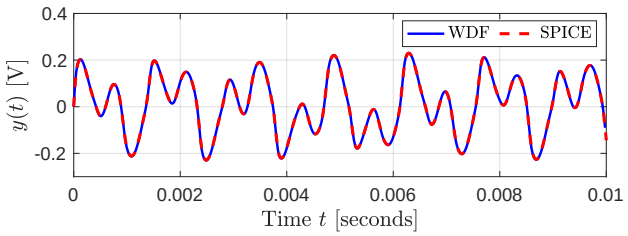

Figure 12: *Comparison between WDF in Figure 10(a) and Spice. Output* $y(t)$ *given input* $u(t) = \sum_{j=1}^{2} g_j \sin(2\pi f_{0j})$ with $g_1 = 0.5$ V, $f_{01} = 650$ Hz, $g_2 = 0.35$ V and $f_{02} = 1450$ Hz.

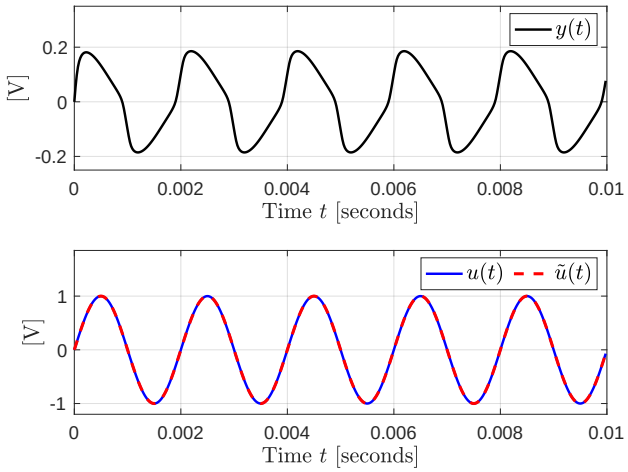

Figure 13: *Results of WDF implementation of master and slave, given a sinusoidal input* $u(t) = \sin(2\pi f_0)$ with $f_0 = 500$ Hz.

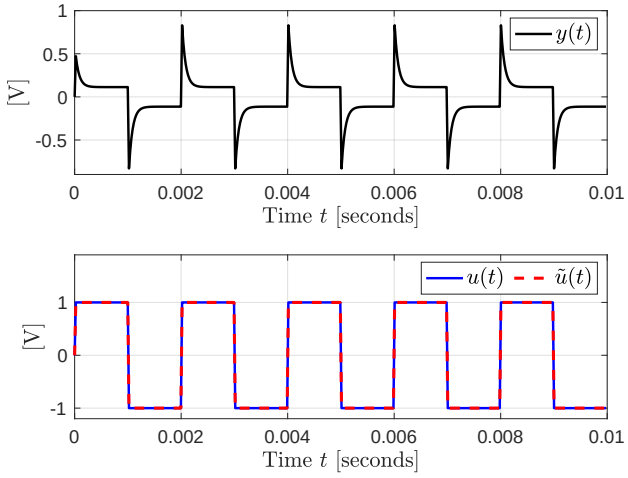

Figure 14: *Results of WDF implementation of master and slave, given a square wave input* $u(t) = \mathrm{sgn}\left(\sin(2\pi f_0)\right)$ with $f_0 = 500$ Hz.

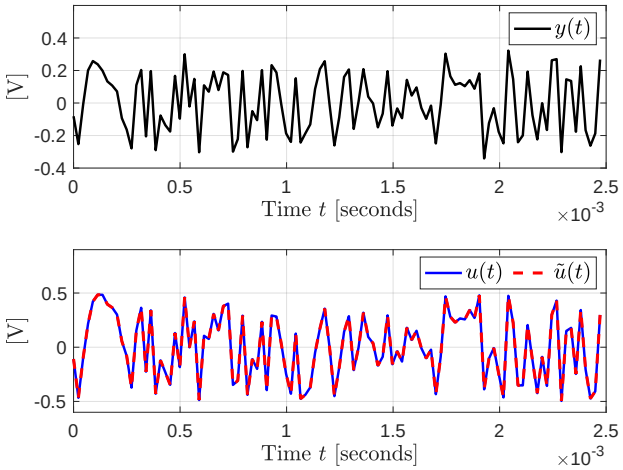

Figure 15: *Results of WDF implementation of master and slave, given a zero-centered white noise with amplitude* 1 *as input.*

MIMO systems and to systems with uncertain parameters.

6. ACKNOWLEDGMENTS

The authors wish to thank Federico Borra and Kurt James Werner for the encouraging discussions about the potential benefits of inverse Virtual Analog modeling in digital audio applications.

7. REFERENCES

[1] J. O. Smith, "Physical modeling synthesis update," *Computer Music Journal*, vol. 20, no. 2, pp. 44–56, 1996.

[2] J. Pakarinen, V. Välimäki, F. Fontana, V. Lazzarini, and J. S. Abel, "Recent advances in real-time musical effects, synthesis, and virtual analog models," *EURASIP J. on Advances in Signal Process.*, vol. 2011, no. 1, pp. 940784, Feb 2011.

[3] Stefano D'Angelo, *Virtual Analog Modeling of Nonlinear Musical Circuits*, Ph.D. Dissertation, Aalto University, Espoo, Finland, Sept. 2014.

[4] T. Helie, "Volterra series and state transformation for real-time simulations of audio circuits including saturations: Application to the moog ladder filter," *IEEE Trans. on Audio, Speech, and Language Processing*, vol. 18, no. 4, pp. 747–759, May 2010.

[5] F. Eichas and U. Zölzer, "Gray-box modeling of guitar amplifiers," *J. Audio Eng. Soc*, vol. 66, no. 12, pp. 1006–1015, 2018.

[6] A. Novak, L. Simon, F. Kadlec, and P. Lotton, "Nonlinear system identification using exponential swept-sine signal," *IEEE Trans. Instrum. Meas.*, vol. 59, no. 8, pp. 2220–2229, Aug 2010.

[7] T. Schmitz and J. J. Embrechts, "Nonlinear real-time emulation of a tube amplifier with a long short time memory neural-network," in *Audio Engineering Society Convention 144*, May 2018.

[8] A. Carini, S. Cecchi, M. Gasparini, and G. L. Sicuranza, "Introducing legendre nonlinear filters," in *IEEE Int. Conf. on Acoustics, Speech and Signal Processing (ICASSP)*, May 2014, pp. 7939–7943.

[9] David T. Yeh, Jonathan S. Abel, and Julius O. Smith, "Automated physical modeling of nonlinear audio circuits for real-time audio effects - part 1: Theoretical development," *IEEE Trans. Audio, Speech, Language Process.*, vol. 18, pp. 728–737, May 2010.

[10] K. Dempwolf, M. Holters, and U. Zölzer, "Discretization of parametric analog circuits for real-time simulations," in *Proc. 13th Conf. Digital Audio Effects*, Graz, Austria, Sept. 42–49 2010.

[11] Antoine Falaize and Thomas Hélie, "Passive guaranteed simulation of analog audio circuits: A port-hamiltonian approach," *Appl. Sci.*, vol. 6, no. 10, 2016.

[12] Alfred Fettweis, "Wave digital filters: Theory and practice," *Proc. IEEE*, vol. 74, no. 2, pp. 270–327, Feb. 1986.

[13] Giovanni De Sanctis and Augusto Sarti, "Virtual analog modeling in the wave-digital domain," *IEEE Trans. Audio, Speech, Language Process.*, vol. 18, pp. 715–727, May 2010.

[14] M. Schetzen, *The Volterra and Wiener Theories of Nonlinear Systems*, Krieger Publishing Co., Inc., Melbourne, FL, USA, 2006.

[15] A. Sarti and S. Pupolin, "Recursive techniques for the synthesis of a pth-order inverse of a volterra system," *European Transactions on Telecommunications*, vol. 3, no. 4, pp. 315–322, 1992.

[16] A. Carini, G. L. Sicuranza, and V. J. Mathews, "On the inversion of certain nonlinear systems," *IEEE Signal Processing Letters*, vol. 4, no. 12, pp. 334–336, Dec 1997.

[17] A. Leuciuc, "The realization of inverse system for circuits containing nullors with applications in chaos synchronization," *International Journal of Circuit Theory and Applications*, vol. 26, no. 1, pp. 1–12, 1998.

[18] H. J. Carlin, "Singular network elements," *IEEE Trans. Circuit Theory*, vol. 11, no. 1, pp. 67–72, Mar. 1964.

[19] K. J. Werner, W. R. Dunkel, M. Rest, M. J. Olsen, and J. O. Smith III, "Wave digital filter modeling of circuits with operational amplifiers," in *Proc. Eur. Signal Process. Conf.*, Budapest, Hungary, Aug. 2016, pp. 1033–1037.

[20] K. J. Werner, A. Bernardini, J. O. Smith, and A. Sarti, "Modeling circuits with arbitrary topologies and active linear multiports using wave digital filters," *IEEE Transactions on Circuits and Systems I: Regular Papers*, vol. 65, no. 12, pp. 4233–4246, Dec 2018.

[21] F. Bohme and W. Schwarz, "The chaotizer-dechaotizer-channel," *IEEE Transactions on Circuits and Systems I: Fundamental Theory and Applications*, vol. 43, no. 7, pp. 596–599, July 1996.

[22] U. Feldmann, M. Hasler, and W. Schwarz, "Communication by chaotic signals: the inverse system approach," *International Journal of Circuit Theory and Applications*, vol. 24, no. 5, pp. 551–579, 1996.

[23] Louis M. Pecora and Thomas L. Carroll, "Synchronization of chaotic systems," *Chaos: An Interdisciplinary Journal of Nonlinear Science*, vol. 25, no. 9, pp. 0976111–09761112, 2015.

[24] A. Bernardini and A. Sarti, "Biparametric wave digital filters," *IEEE Trans. Circuits Syst. I, Reg. Papers*, vol. 64, no. 7, pp. 1826–1838, July 2017.

[25] D. Rocchesso and J. O. Smith, "Generalized digital waveguide networks," *IEEE Trans. on Speech and Audio Process.*, vol. 11, no. 3, pp. 242–254, May 2003.

[26] Augusto Sarti and Giovanni De Poli, "Toward nonlinear wave digital filters," *IEEE Trans. Signal Process.*, vol. 47, pp. 1654–1668, June 1999.

[27] Rafael C. D. Paiva, Stefano D'Angelo, Jyri Pakarinen, and Vesa Välimäki, "Emulation of operational amplifiers and diodes in audio distortion circuits," *IEEE Trans. Circuits Syst. II, Exp. Briefs*, vol. 59, pp. 688–692, Oct. 2012.

[28] K. J. Werner, J. O. Smith, and J. S. Abel, "Wave digital filters adaptors for arbitrary topologies and multiport linear elements," in *Proc. 18th Conf. Digital Audio Effects*, Trondheim, Norway, Nov. 30 – Dec. 3 2015.

[29] M. Verasani, A. Bernardini, and A. Sarti, "Modeling sallen-key audio filters in the wave digital domain," in *2017 IEEE International Conference on Acoustics, Speech and Signal Processing (ICASSP)*, March 2017, pp. 431–435.

[30] Ó. Bogason and K. J. Werner, "Modeling circuits with operational transconductance amplifiers using wave digital filters," in *Proc. 20th Int. Conf. Digital Audio Effects*, Edinburgh, UK, Sept. 2017, pp. 130–137.

[31] Rafael Cauduro Dias de Paiva, Jyri Pakarinen, Vesa Välimäki, and Miikka Tikander, "Real-time audio transformer emulation for virtual tube amplifiers," *EURASIP J. on Advances in Signal Process.*, Jan. 2011.

[32] A. Bernardini, K. J. Werner, A. Sarti, and J. O. Smith, "Multi-port nonlinearities in wave digital structures," in *Proc. IEEE Int. Symp. Signals Circuits Syst.*, Iasi, Romania, July 9–10 2015.

[33] K. J. Werner, V. Nangia, A. Bernardini, J. O. Smith III, and A. Sarti, "An improved and generalized diode clipper model for wave digital filters," in *Proc. 139th Conv. Audio Eng. Soc. (AES)*, New York, NY, Oct. 2015, conv. paper #9360.

[34] A. Bernardini and A. Sarti, "Canonical piecewise-linear representation of curves in the wave digital domain," in *Proc. 25th Eur. Signal Proces. Conf. (EUSIPCO)*, Aug. 2017, pp. 1125–1129.

[35] J. Pakarinen and M. Karjalainen, "Enhanced wave digital triode model for real-time tube amplifier emulation," *IEEE Transactions on Audio, Speech, and Language Processing*, vol. 18, no. 4, pp. 738–746, May 2010.

[36] Stefano D'Angelo, Jyri Pakarinen, and Vesa Välimäki, "New family of wave-digital triode models," *IEEE Trans. Audio, Speech, Language Process.*, vol. 21, pp. 313–321, Feb. 2013.

[37] A. Bernardini, K. J. Werner, A. Sarti, and J. O. Smith, "Modeling a class of multi-port nonlinearities in wave digital structures," in *Proc. European Signal Process. Conf. (EUSIPCO)*, Nice, France, Aug. 31 – Sept. 4 2015, pp. 669–673.

[38] K. J. Werner, V. Nangia, J. O. Smith, and J. S. Abel, "Resolving wave digital filters with multiple/multiport nonlinearities," in *Proc. 18th Conf. Digital Audio Effects*, Trondheim, Norway, Nov. 30 – Dec. 3 2015.

[39] A. Bernardini, K. J. Werner, A. Sarti, and J. O. Smith III, "Modeling nonlinear wave digital elements using the Lambert function," *IEEE Trans. Circuits Syst. I, Reg. Papers*, vol. 63, no. 8, pp. 1231–1242, Aug. 2016.

[40] Michael Jørgen Olsen, Kurt James Werner, and J. O. Smith, "Resolving grouped nonlinearities in wave digital filters using iterative techniques," in *Proc. 19th Int. Conf. Digital Audio Effects*, Brno, Czech Republic, September 5–9 2016, pp. 279–286.

[41] D. Hernandez and J. Huang, "Emulation of junction field-effect transistors for real-time audio applications," *IEICE Electronics Express*, May 2016.

[42] A. Bernardini, K. J. Werner, J. O. Smith, and A. Sarti, "Generalized wave digital filter realizations of arbitrary reciprocal connection networks," *IEEE Trans. Circuits and Systems I: Regular Papers*, vol. 66, no. 2, pp. 694–707, Feb 2019.

[43] Klaus Meerkötter and Reinhard Scholz, "Digital simulation of nonlinear circuits by wave digital filter principles," in *IEEE Int. Symp. Circuits Syst.*, June 1989, pp. 720–723.

[44] G. Borin, G. De Poli, and D. Rocchesso, "Elimination of delay-free loops in discrete-time models of nonlinear acoustic systems," *IEEE Trans. Speech Audio Process.*, vol. 8, no. 5, pp. 597–605, Sept. 2000.

[45] Timothy Schwerdtfeger and Anton Kummert, "Newton's method for modularity-preserving multidimensional wave digital filters," in *Proc. IEEE Int. Work. Multidimensional Syst.*, Vila Real, Portugal, Sept. 2015.

[46] Alberto Bernardini, Paolo Maffezzoni, Luca Daniel, and Augusto Sarti, "Wave-based analysis of large nonlinear photovoltaic arrays," *IEEE Trans. Circuits Syst. I, Reg. Papers*, vol. 65, no. 4, pp. 1363–1376, Apr. 2018.

[47] Alberto Bernardini, Augusto Sarti, Paolo Maffezzoni, and Luca Daniel, "Wave digital-based variability analysis of electrical mismatch in photovoltaic arrays," in *Proc. IEEE Int. Symposium on Circuits and Systems (ISCAS)*, Florence, Italy, May 27–30 2018.

[48] Alberto Bernardini, Kurt James Werner, Paolo Maffezzoni, and Augusto Sarti, "Wave digital modeling of the diode-based ring modulator," in *Proc. 144nd Conv. Audio Eng. Soc.*, Milan, Italy, May 2018, conv. paper #10015.

[49] C. W. Ho, A. E. Ruehli, and P. A. Brennan, "The modified nodal approach to network analysis," *IEEE Trans. Circuits Syst.*, vol. 22, no. 6, pp. 504–509, June 1975.